Hindawi
Shock and Vibration
Volume 2020, Article ID 8857947, 12 pages
https://doi.org/10.1155/2020/8857947

Research Article

Simulation Study on the Effect of Forced Ventilation in Tunnel under Single-Head Drilling and Blasting

Qingsong Pu,[1,2,3] **Yi Luo**,[1] **Junhong Huang**,[1,2,4] **Yingwei Zhu**,[4] **Shaohua Hu**,[4] **Chenhao Pei**,[1,2] **Guang Zhang**,[4] **and Xinping Li**[1]

[1]*Hubei Key Laboratory of Roadway Bridge and Structure Engineering, Wuhan University of Technology, Wuhan, China*
[2]*School of Civil Engineering and Architecture, Wuhan University of Technology, Wuhan, China*
[3]*China Railway No. 5 Engineering Group Co., Ltd., Guiyang, China*
[4]*School of Safety Science and Emergency Management, Wuhan University of Technology, Wuhan, China*

Correspondence should be addressed to Yi Luo; yluo@whut.edu.cn and Junhong Huang; junhonghuang@whut.edu.cn

Received 19 March 2020; Revised 29 August 2020; Accepted 22 October 2020; Published 5 November 2020

Academic Editor: Mohammad Rafiee

Copyright © 2020 Qingsong Pu et al. This is an open access article distributed under the Creative Commons Attribution License, which permits unrestricted use, distribution, and reproduction in any medium, provided the original work is properly cited.

Based on the excavation of Yuelongmen tunnel on ChengLan Railway in China, this paper will probe into the forced ventilation effect of harmful gas generated by drilling and blasting construction, simulate the diffusion process of harmful gas generated during blasting operation on the tunnel face by establishing the finite element model of gas turbulent flow and concentration diffusion in the tunnel, and study the spatial-temporal evolution law of CO concentration field under different air pipe layout locations and tunnel excavation methods. The results show that, compared with corner layout, haunch layout, and central layout, the ventilation effect is the best when the air pipes are arranged near the wall at the tunnel vault, and the CO concentration can be reduced to the concentration limit after 588 s of ventilation; compared with the full-face tunneling method and the lower pilot heading method, the benching tunneling method can effectively reduce the retention time of CO near the tunnel face, and the CO concentration on the tunnel face can be reduced to the standard limit after 326 s of ventilation near the wall of tunnel vault.

1. Introduction

With the continuous construction of the railway network in southwest China, tunnels have become the key works of the railway network in southwest China due to geographical limitation, such as mountainous and hilly areas. Owing to its simple, efficient, and economical construction method, drilling and blasting is the main tunnel construction method for hard rock mass at present [1], but a large amount of harmful gas, such as CO, will lead to the suffocation of constructors and even tunnel explosion after blasting [2, 3]. Therefore, it is of great significance to study the concentration distribution law of CO and other harmful gas in the tunnel and reasonably set up the tunnel ventilation system, so as to ensure the occupational health of construction workers, as well as construction safety and project progress [4–6].

Tunnel construction ventilation is to send fresh air near the tunnel face by means of natural ventilation or mechanical ventilation, so as to dilute and reduce the concentration of harmful gas below the allowable concentration, which is the only technical means of air exchange inside and outside the tunnel [7, 8]. At present, the research methods on the ventilation and discharge of harmful gas from tunnel implosion can be divided into field measurement, model test, theoretical analysis, and numerical simulation [9]. Nevertheless, the occurrence of the field measured flow phenomenon is not controllable, and it is difficult to summarize the fluid movement rule based on the measured data [10]. The model test is to transform the test data into actual prototype data based on the similarity theory, but it often takes a long operation cycle and high cost [11, 12]. Theoretical analysis can only be used to solve some simple hydrodynamic problems, but it is difficult to solve 3D

hydrodynamic problems of tunnel construction ventilation [13–15]. Numerical simulation has been widely used for its advantages of low cost, strong operability, and fast simulation results [16–18].

Because of the complex engineering geological conditions and hydrogeological conditions in southwest China, the full-face tunneling method can no longer meet the requirements of tunnel construction in this region, and the relevant research work on ventilation problems in other construction methods is relatively insufficient [19–21]. The difference in space structure at the tunnel face caused by different construction methods makes it more difficult to predict the diffusion process and distribution characteristics of harmful gas [22, 23]. Due to the complexity of ventilation problems, the existing ventilation experience of a single-head tunnel with full section drilling and blasting excavation cannot meet the ventilation requirements of other construction methods. Based on HD3K0 + 148 section of No. 3 horizontal tunnel of Yuelongmen tunnel of Chenglan Railway in China, this paper studied the influence of air pipe layout and tunnel excavation on the ventilation effect of explosive harmful gas and put forward the corresponding optimization measures.

2. Numerical Model of Forced Ventilation for Tunnel Construction with Single-Head Drilling and Blasting

2.1. Fundamental Assumption. The forced ventilation of tunnel under single-head drilling and blasting construction is a typical turbulent flow problem in fluid dynamics. The source of harmful gas in the tunnel is the explosive gas, which is distributed evenly on the tunnel face. The temperature in the tunnel is constant, the tunnel wall is adiabatic, and the dissipative heat caused by fluid viscous force is ignored. In addition to the air pipes, the influence of other equipment in the tunnel on the flow field is ignored [24].

2.2. Governing Equation. The airflow model based on the Navier–stokes equation is employed for tunnel construction, and the equations are closed by using the RNG $k-\varepsilon$ turbulence model. The control equations of gas turbulent flow and concentration diffusion in the tunnel are as follows:

(1) Continuity equation:

$$\frac{\partial \rho}{\partial t} + \frac{\partial}{\partial x_i}\left(\rho v_i\right) = 0, \tag{1}$$

where ρ is the gas density, v_i is the speed in x_i direction, t is the ventilation time.

(2) Momentum conservation equation:

$$\frac{\partial}{\partial t}\left(\rho v_i\right) + \frac{\partial}{\partial x_i}\left(\rho v_i v_j\right) = -\frac{\partial p}{\partial x_i} + \rho f_{x_i} + \frac{\partial \tau_{ij}}{\partial x_i}, \tag{2}$$

where p is the static pressure, τ_{ij} is the viscous stress component, and f_{xi} is the gravity body force and external body force in i direction.

(3) Energy conservation equation:

$$\frac{\partial}{\partial t}\left(\rho T\right) + \frac{\partial}{\partial x_i}\left(\rho v_i T\right) = \sum \frac{\partial}{\partial x_i}\left(\frac{K}{c_p}\frac{\partial T}{\partial x_i}\right) + S_T, \tag{3}$$

where T is temperature, K is the heat transfer coefficient of fluid, c_p is the specific heat capacity, and S_T is the viscous dissipation.

(4) Component mass conservation equation:

$$\frac{\partial}{\partial t}\left(\rho c_s\right) + \frac{\partial}{\partial x_i}\left(\rho c_s v_i\right) = \frac{\partial}{\partial x_i}\left(D_s \frac{\partial}{\partial x_i}\left(\rho c_s\right)\right), \tag{4}$$

where c_s is the mass concentration of a component, and D_s is the diffusion coefficient of the component.

Due to the fact that tunnel construction ventilation is often accompanied by the flow on the curved wall, RNG $k-\varepsilon$ turbulence model is introduced to calculate the turbulent flow with a high strain rate and greater curvature in the tunnel. The transport equations for k and ε are, respectively:

$$\frac{\partial}{\partial t}\left(\rho k\right) + \frac{\partial}{\partial x_i}\left(\rho k v_i\right) = \frac{\partial}{\partial x_i}\left(\alpha_k u_{\text{eff}} \frac{\partial k}{\partial x_j}\right) + G_k - \rho\varepsilon,$$

$$\frac{\partial}{\partial t}\left(\rho \varepsilon\right) + \frac{\partial}{\partial x_i}\left(\rho \varepsilon v_i\right) = \frac{\partial}{\partial x_i}\left(\alpha_\varepsilon u_{\text{eff}} \frac{\partial \varepsilon}{\partial x_j}\right) + \frac{C_{1\varepsilon}^*}{k} G_k - C_{2\varepsilon}\rho\frac{\varepsilon^2}{k}, \tag{5}$$

where μ_{eff} is the effective viscosity coefficient, G_k is the turbulent kinetic energy production term caused by average speed gradient, k is the turbulent kinetic energy, and ε is the turbulence dissipation rate. $C_{1\varepsilon}^*, C_{2\varepsilon}, \alpha_k, \alpha_\varepsilon$ are the model constants, $C_{1\varepsilon}^* = 1.42$, $C_{2\varepsilon} = 1.68$, and $\alpha_k = \alpha_\varepsilon = 1.39$.

3. Finite Element Model and Working Condition Design

3.1. Finite Element Modeling. CFD business software FLUENT can be used to simulate complex flows from incompressible to highly compressible range. Its flexible unstructured grid and solution-based adaptive grid technology and mature physical models make FLUENT transform and turbulent. It is widely used in heat transfer and phase change, chemical reaction and combustion, and multiphase flow.

The clearance size of HD3K0 + 148 section of No. 3 horizontal tunnel of Yuelongmen Tunnel is 7.65 m (wide) × 6.85 m (high), the section area is 47.68 m^2, and the surrounding rock of the tunnel face is carbonic phyllite, as shown in Figure 1. The air pipe is suspended in the near-wall area with a radius of 0.75 m. The tunnel and air pipe model of this section are shown in Figure 2. The established numerical model contains 229,900 nodes and 241,480 elements.

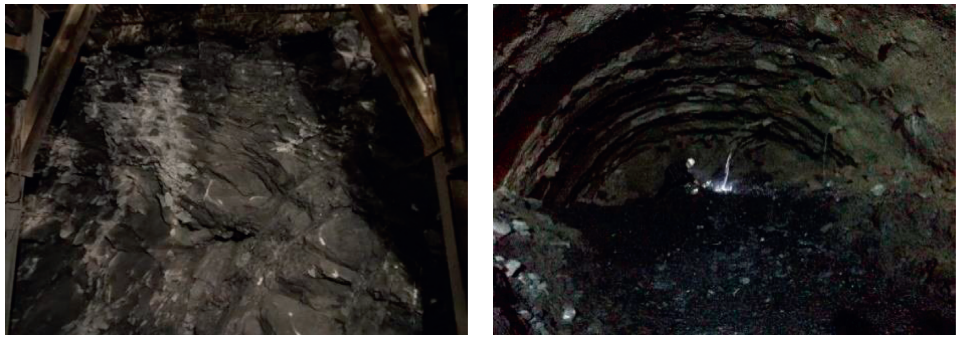

(a) (b)

Figure 1: Tunnel face of HD3K0 + 148 section.

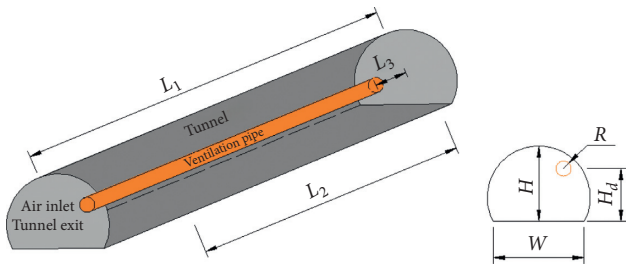

L_1 = 100 m, L_2 = 72 m, L_3 = 15 m, W = 7.65 m, H = 6.85 m, R = 075 m

L_1 is the simulated ventilation length of the tunnel;

L_2 is the throwing length of CO;

L_3 is the distance from the air duct outlet to the tunnel face;

W is the width of the tunnel;

H_d is the air duct layout height;

R is the radius of air duct.

Figure 2: Tunnel model size design.

3.2. Initial Conditions of Explosion Gas and Tunnel Boundary Conditions

3.2.1. Initial Conditions for Explosion Gas. After the completion of blasting operation in tunnel construction, the content of CO in the explosion gas is about 70%, the content of NO_x and SO_2 is about 20%, and there is a small amount of H_2S, HCl, and so forth, except CO, SO_2, H_2S, and HCl cannot exist in the tunnel space steadily due to physical and chemical properties, and the CO content is the largest. Therefore, CO dilution and emission condition is used in this paper to measure the ventilation effect of the tunnel [25].

It is assumed that the temperature immediately returns to the average temperature of 19°C in the tunnel after the blasting operation is completed, and the CO gas generated is evenly distributed in the throwing space. The empirical formula of blasting fume throwing is

$$L = 15 + \frac{G}{5}, \tag{6}$$

where L is the throwing length of blasting fume, namely, the length of the diffused area of blasting fume (m); G is the amount of blasting explosive (kg).

The formula for calculating the initial concentration of CO is

$$C = \frac{Gb}{LA}, \tag{7}$$

where C is the initial concentration of CO; b is the toxic gas (m^3/kg) generated by each kilogram of explosives, 0.04; and A is the tunnel construction section area (m^2).

According to the tunnel surrounding rock classification and daily construction schedule, the amount of explosive in a single blasting operation is 63 kg, producing a total of 929.76 L CO gas, and the throwing length of blasting fume is 27.6 m, so the average initial concentration of CO is 903 mg/m^3.

3.2.2. Tunnel Boundary Condition. The inner wall of the tunnel is the standard solid wall boundary, and the wall roughness function is as follows:

$$\Delta B = \frac{1}{\kappa}\ln\left(1 + C_s K_s\right), \tag{8}$$

where κ is the empirical constant, 0.4; No. 3 horizontal tunnel of Yuelongmen Tunnel has been lined for the first time to HD3K0 + 128 section, the wall surface of the lined support section is uniform concrete sand surface, with the roughness constant $C_{s1} = 0.5$, the rough particle height $K_{s1} = 0.09$; the wall surface of unsupported section is bare rock, with the roughness constant $C_{s2} = 0.7$, and the rough particle height $K_{s2} = 0.3$ [26–28].

The tunnel face is equipped with a 2 × 200 kw SDF (B)-6-No18 ventilator, which can provide the air volume of 5792 m^3/min, and the pipe inlet is a constant speed boundary condition, with the radius R = 0.75 m, and the outlet wind speed of 13.2 m/s.

The tunnel exit pressure is assumed to be 1.01325×10^5 Pa, and the free exit boundary condition is adopted. The normal gradient of all flow parameters is 0 except for the pressure at the tunnel exit surface.

3.3. Operation Condition Design

3.3.1. Different Air Pipe Layout Modes. According to the Technical Guide for Railway Tunnel Engineering Construction (TZ204-2008) [29], the air pipe is generally laid in the central vault, the middle of the tunnel, or beside the haunch and corner, as shown in Figure 3, in which Point A is the monitoring point of CO concentration on the tunnel face, and the monitoring period is the change of CO concentration near the tunnel face within 30 min after blasting.

3.3.2. Different Tunnel Construction Methods. Different tunnel construction methods also have a great influence on the diffusion of CO concentration. In addition to the full-section construction method adopted at the present stage, both the step-construction method and lower pilot heading construction method are applicable to this section. The step-construction method and lower pilot heading method are shown in Figures 4 and 5. In this paper, the influence of different tunnel construction methods on CO concentration distribution characteristics under the same simulation condition is discussed by taking the full-section method, benching tunneling method, and lower pilot heading method as examples.

4. Numerical Simulation Analysis of Forced Ventilation of Tunnel

4.1. Influence of Air Pipe Layout on CO Diffusion Law. Figure 6 shows the variation curve of CO ventilation diffusion concentration at A on the tunnel face. After the single-head tunneling and blasting construction, the change of CO concentration near the tunnel face can be divided into three stages. Stage I: 5 min before ventilation, CO rapidly diffuses from the tunnel face to the middle of the tunnel under the effect of fresh jet air dilution, and CO concentration decreases most rapidly at this moment. Stage II: ventilation for 5 min~15 min, the residual CO near the tunnel face is continuously diluted under the action of jet air and vortex wind inside the tunnel, during which the decline rate of CO concentration decreases continuously until the CO concentration on the tunnel face decreases to the standard limit. Stage III: after 15 min of ventilation, there is a very small amount of CO remaining near the tunnel face, and the decline rate of CO concentration is gradually close to 0, until the CO near the tunnel face is completely diluted and eliminated. When the air pipe is laid at the vault near the tunnel wall, the time required to reduce the CO concentration to the standard limit is 588 s. However, it will take 738 s, 840 s, and 786 s to reduce the CO concentration to the standard limit when the air pipe is laid at the corner, haunch, and center of the tunnel, respectively. The numerical simulation results are close to the monitoring results, and the rules are similar, indicating that this numerical model can effectively reflect the dilution process of the CO concentration in the tunnel.

Since the CO concentration on the tunnel face can reach the standard limit of 20 mg/m^3 within 900 s under different air pipe layout conditions [30], the CO concentration distribution in the tunnel cross section after ventilation for 300 s, 600 s, and 900 s on the tunnel face ventilation is analyzed, as shown in Figure 7.

(1) When the air pipe is laid at the corner close to the tunnel wall (as shown in Figure 7(a)), the high-concentration CO area appears on the tunnel face opposite to the air pipe, and the distribution height of the high-concentration area is similar to the suspension height of the air pipe. With the increase of ventilation time, the area of high-concentration CO keeps decreasing and the concentration keeps decreasing. The maximum CO concentration corresponding to ventilation for 300 s, 600 s, and 900 s is 151.2 mg/m^3, 39.2 mg/m^3, and 11.2 mg/m^3, respectively.

(2) When the air pipe is laid near the haunch of the tunnel wall (as shown in Figure 7(b)), the area with high CO concentration appears on the tunnel face at the lower left of the air pipe, and the highest CO concentration at different periods is 156.8 mg/m^3, 49.0 mg/m^3, and 17.4 mg/m^3, respectively.

(3) When the air pipe is laid in the middle of the tunnel (as shown in Figure 7(c)), the low concentration of CO appears on the tunnel face at the pipe orifice, with the distribution pattern similar to a concentric circle, and CO concentration is increased continuously along the side and reaches the highest concentration at the intersection between the tunnel bottom and inner tunnel wall, with the highest CO concentrations at different times of 134.4 mg/m^3, 30.8 mg/m^3, and 7.3 mg/m^3, respectively.

(4) When the air pipe is arranged near the vault of the tunnel wall (as shown in Figure 7(d)), the high concentration of CO appears at the tunnel bottom, and the highest concentration of CO is 81.2 mg/m^3, 10.6 mg/m^3, and 1.5 mg/m^3, respectively. The distribution range is small, the distribution of CO concentration on the tunnel face above the tunnel is relatively uniform, and the difference of CO concentration between adjacent positions is not large.

After comparing the CO concentration distribution and changes under different air duct layout methods, it was found that when the air duct is laid near the arch of the tunnel near the wall, the CO concentration distribution on the palm face is more uniform, and it is easy to accumulate at

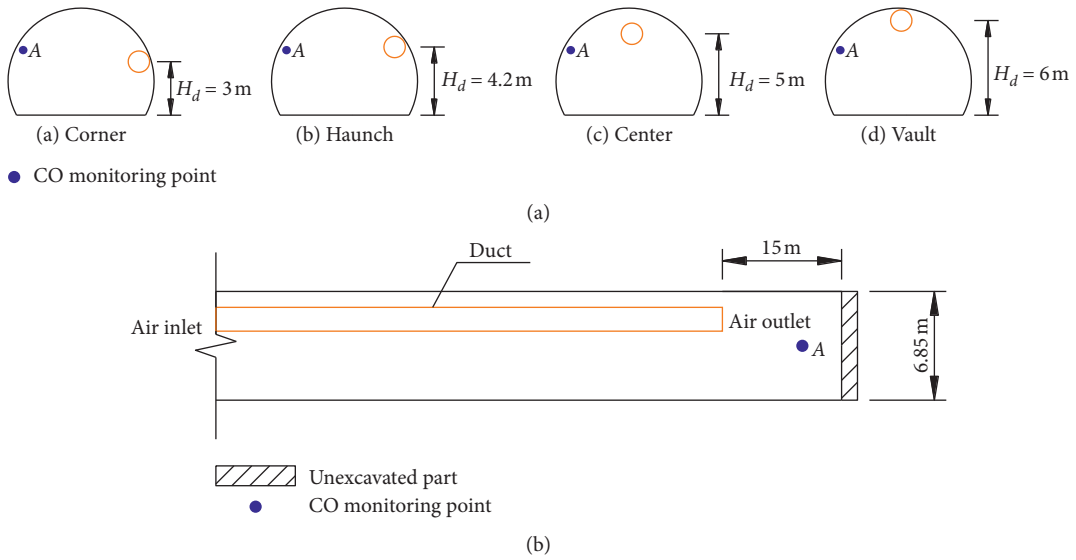

Figure 3: Indication of simulated cross section and longitudinal section for air pipe layout. (a) Cross section. (b) Longitudinal section.

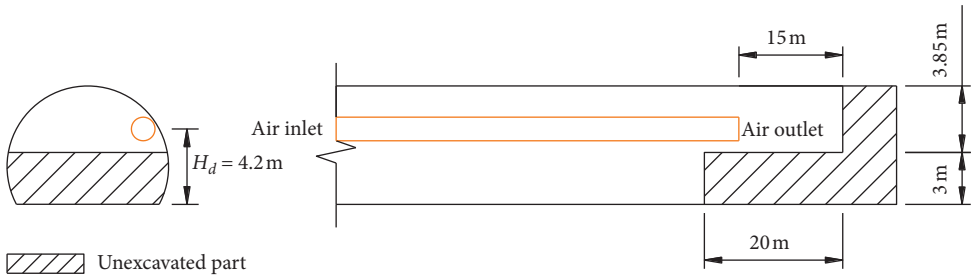

Figure 4: Ventilation diagram of the benching tunneling method.

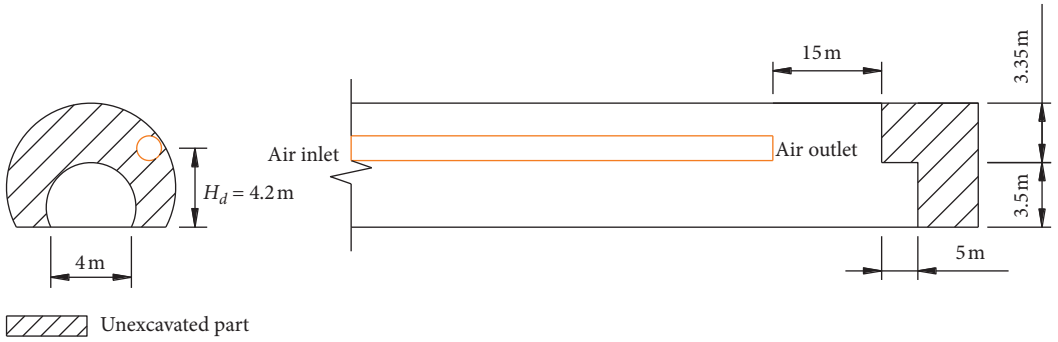

Figure 5: Schematic diagram of ventilation under the lower pilot heading method.

the bottom of the tunnel. Therefore, the air pipe layout here is conducive to the occupational health of tunnel construction and construction personnel.

In addition, under different air pipe layout conditions, the CO concentration in the tunnel face reaches a stable state within 1800 s. The distribution of CO concentration in the longitudinal section of the tunnel in the tunnel face after ventilation for 600 s, 1200 s, and 1800 s is analyzed, as shown in Figure 8. By comparing different time periods, it can be seen that when the air pipe is laid near the wall (as shown in Figures 8(a), 8(b), and 8(d)), the occurrence state of CO in the tunnel can be divided into two stages with the increase of the distance from the tunnel face.

In the first stage, namely, the section near the tunnel face, when the fresh jet air moves to the face, it is obstructed and forms the impinging jet. Therefore, the direction of air blow organization on the other side of the tunnel fan is changed, and the wind speed on this side is lower than that on the

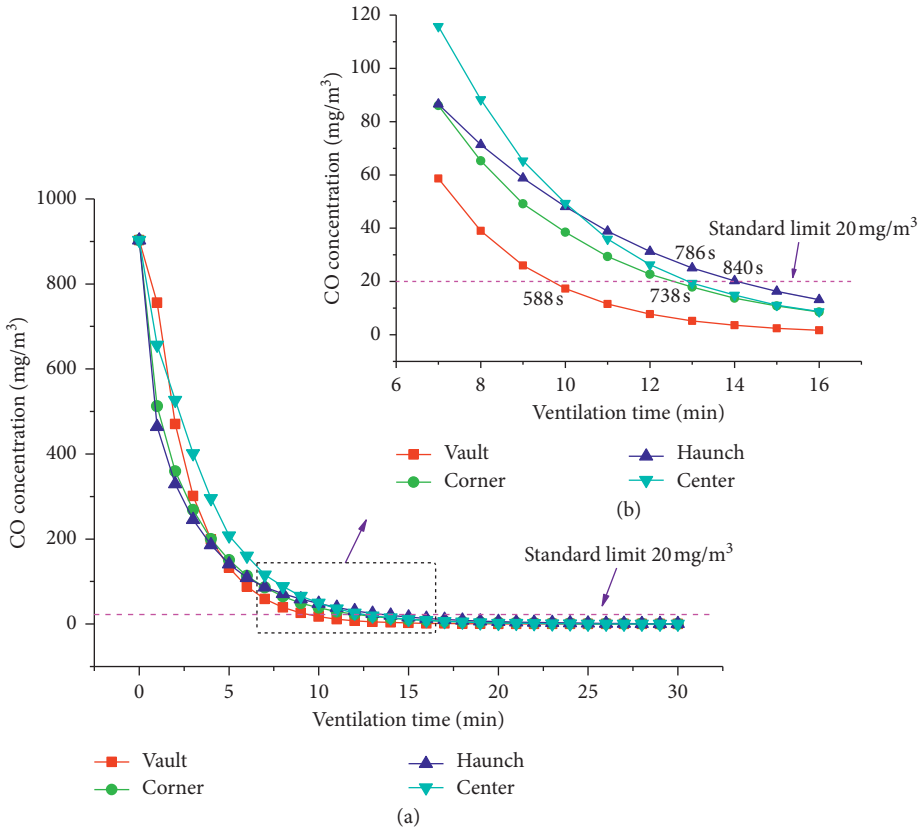

Figure 6: CO ventilation diffusion concentration curve at the point a of the face after blasting.

wind tube. Due to the different air blow organization speed on both sides of the tunnel, CO in this stage is mainly accumulated in the other side of the fan and gradually discharged out of the tunnel.

In the second stage, namely, the section far away from the tunnel face, as the movement of air blow organization in this section is continuously subjected to the impinging jet at the face section and the movement of air blow organization is obstructed by the air pipe, it is difficult to reach the gap between the inner wall of the tunnel and the air pipe. Therefore, CO is detained and accumulated in the gap between the inner wall of the tunnel and the air pipe, and finally discharged out of the tunnel.

When the air pipe is laid in the center (as shown in Figure 8(c)), CO will not gather at the gap between the inner wall of the tunnel and the air pipe, but the detention time of CO in the tunnel will increase due to the lower air pipe position.

4.2. Influence of Tunnel Construction Modes on CO Diffusion Rule. If the air pipe is laid near the wall at the tunnel vault for ventilation, the variations of CO concentration on the tunnel face under different construction methods are shown in Figure 9, in which you can see the CO concentration on the tunnel face in the benching tunneling method is decreased to the standard limit of 20 mg/m^3 after ventilation for 326 s, while it will take 874 s and 784 s for the full-face tunneling method and lower pilot heading method. Due to the smaller space in the benching stage of the benching tunneling method, the influence of airflow on the tunnel face of this section is stronger, which is conducive to the dilution and discharge of CO near the tunnel face. Therefore, the ventilation time is shorter than that of the full-face tunneling method and the lower pilot heading method.

By comparing the full-face tunneling method and lower pilot heading method, it is found that CO concentration declines in the same way at the initial ventilation stage under the two construction methods, and then the air at the tunnel face will continuously flow into the heading section of the lower pilot tunnel as the ventilation time increases, so that the CO concentration on the tunnel face in the lower pilot heading method declines more slowly than that in the full-face tunneling method at some ventilation stages, and the air at the heading stage of the lower pilot tunnel will flow back to the tunnel face after continuous ventilation, so as to promote the dilution of CO, thus making the decrease of CO concentration on the tunnel face slightly faster than that in the full-face tunneling method.

As can be seen from Figure 10, CO is prone to gather in the gap between the inner wall of the tunnel and the air pipe

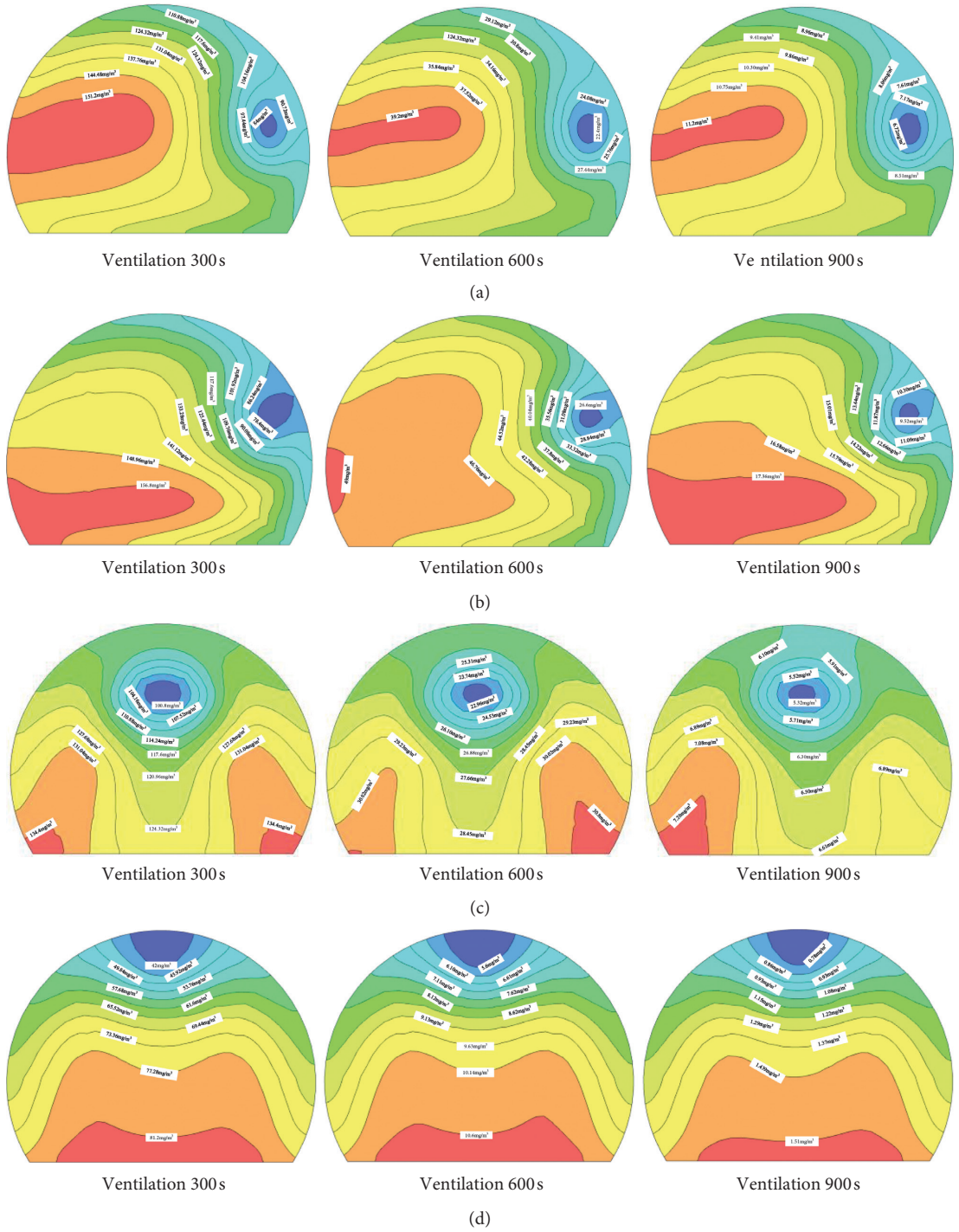

Figure 7: Cloud diagram of CO ventilation diffusion concentration change on the tunnel face after blasting. (a) Corner. (b) Haunch. (c) Center. (d) Vault.

after ventilation in the full-face tunneling method, and the highest concentration after ventilation for 1800 s is 224 mg/m^3. But, compared with the full-face tunneling method, the highest CO concentration in the detention area in the lower pilot heading method is significantly decreased. The highest CO concentration after ventilation for 1800 s is 30.8 mg/m^3. If the benching tunneling method is used, the highest CO concentration after ventilation for 1800 s is the same as that of the lower pilot heading method. However, CO is distributed evenly in the tunnel without any retention and accumulation phenomenon, which is favorable for the elimination of CO.

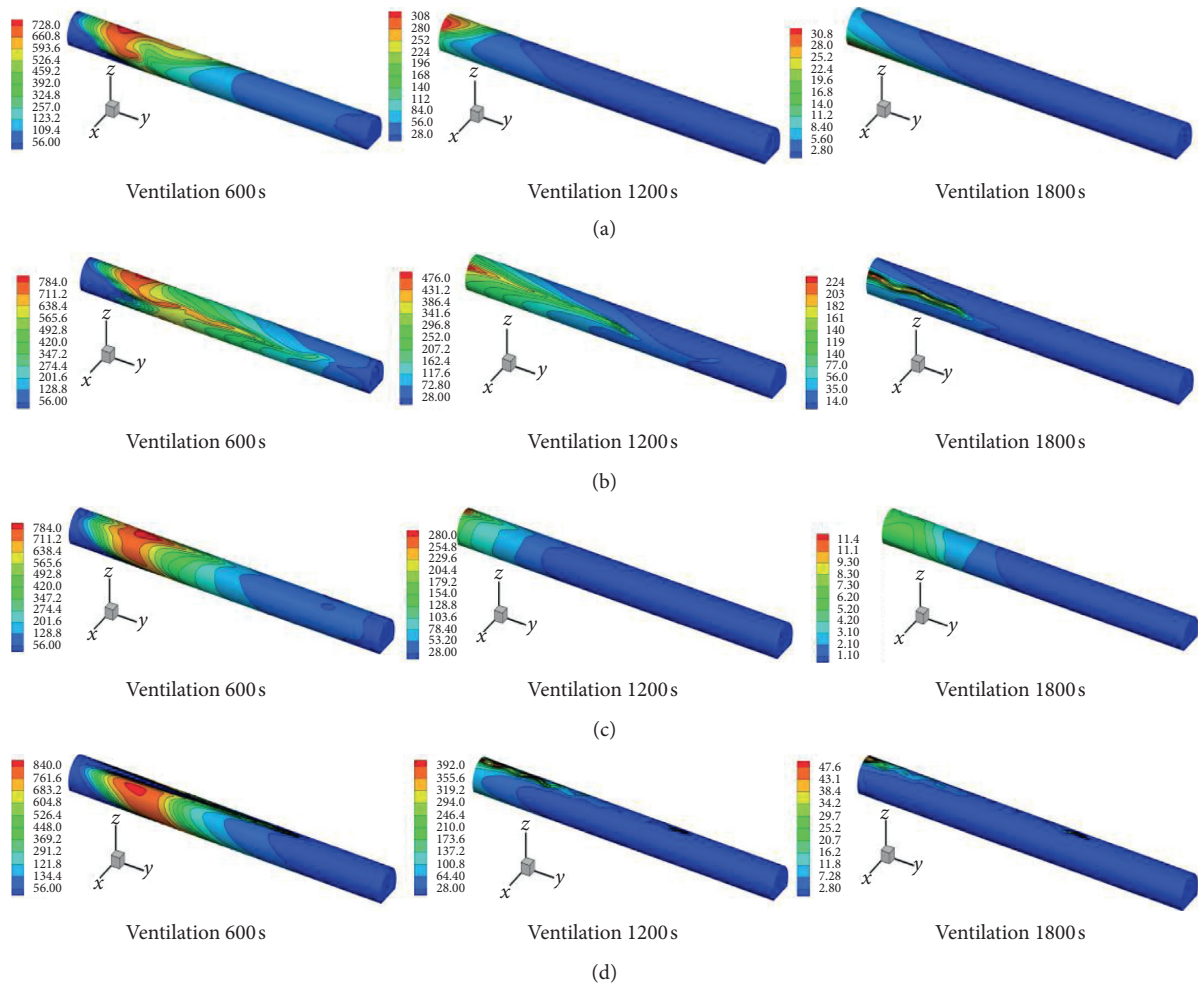

Figure 8: Influence of pipe setting on CO diffusion characteristics (mg/m^3). (a) Corner. (b) Haunch. (c) Center. (d) Vault.

4.3. Influence of Airflow Structure on Working Face. Figure 11 shows the effect of tunnel construction on CO diffusion characteristics. When using the step method (as shown in Figure 11(b)), when ventilating for 300 s, CO is mainly concentrated in the space 50 to 60 m away from the face of the palm, and the highest CO concentration is less than the other two construction methods. The safe area has appeared on the subface. When ventilated for 600 s, the CO concentration of the palm surface of the upper step has basically met the construction requirements, but the CO concentration of the palm surface of the lower step is higher than that of the surrounding space. When ventilating for 900 s , the expansion of the safety space on the palm surface of the upper step is smaller, and the CO concentration on the palm surface of the upper step is reduced, but it does not meet the construction needs. When using the down-lead tunnel construction method (as shown in Figure 11(c)), the CO occurrence in the 600 before ventilation is similar to the full-section method construction, but when the ventilation is 900 s, most of the 25 m space in front of the palm is in the area CO concentration is lower than 20 mg/m^3.

The maximum concentration after full-section construction for 900 s after ventilation is 476 mg/m^3, and the step construction and the leading tunnel construction are 336 mg/m^3 and 420 mg/m^3, respectively. Compared with the three construction methods, the step method construction makes the dead space of the palm surface of the lower step exist, but the overall CO concentration in the tunnel is lower than that of the full-section method. In the later stage of ventilation, the CO concentration in most areas of the palm face space was lower than 20 mg/m^3 by the advanced method of the lower guide tunnel. In summary, step-construction ventilation has the best effect on CO dilution.

Due to the different spatial structure of the tunnel under different construction methods, the airflow structure in the tunnel is changed, which ultimately leads to differences in the CO dilution effect on the palm face. Therefore, it is necessary to analyze the differences of the wind flow structure near the palm face under the three construction methods. It can be seen from Figure 11 that the difference in the CO occurrence state at the palm face under each construction method is caused by the vortex in front of the palm. When the full-section method is used for construction (as shown in Figure 11(a)), there is a vortex zone 2 to 7 m in front of the palm, which causes CO to stay in front of the palm in the early stage of ventilation. When using the step

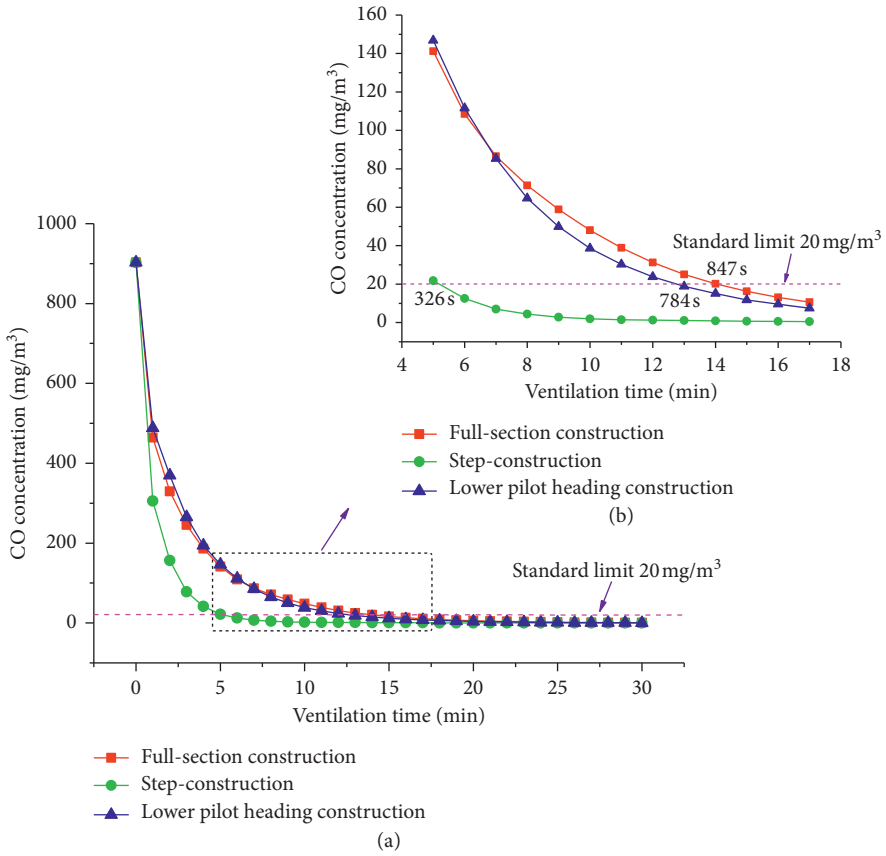

Figure 9: Variation curve of CO ventilation diffusion concentration at A of the tunnel face after blasting.

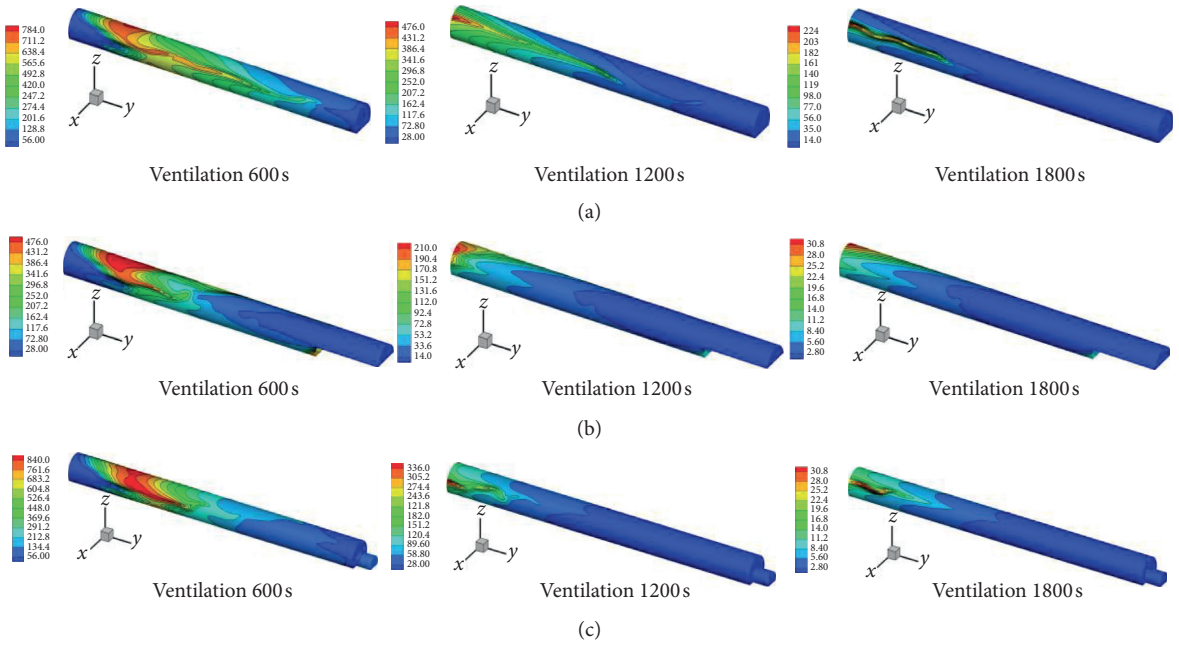

Figure 10: Influence of tunnel construction mode on CO diffusion characteristics (mg/m^3). (a) Full-section construction. (b) Step-construction. (c) Lower pilot heading construction.

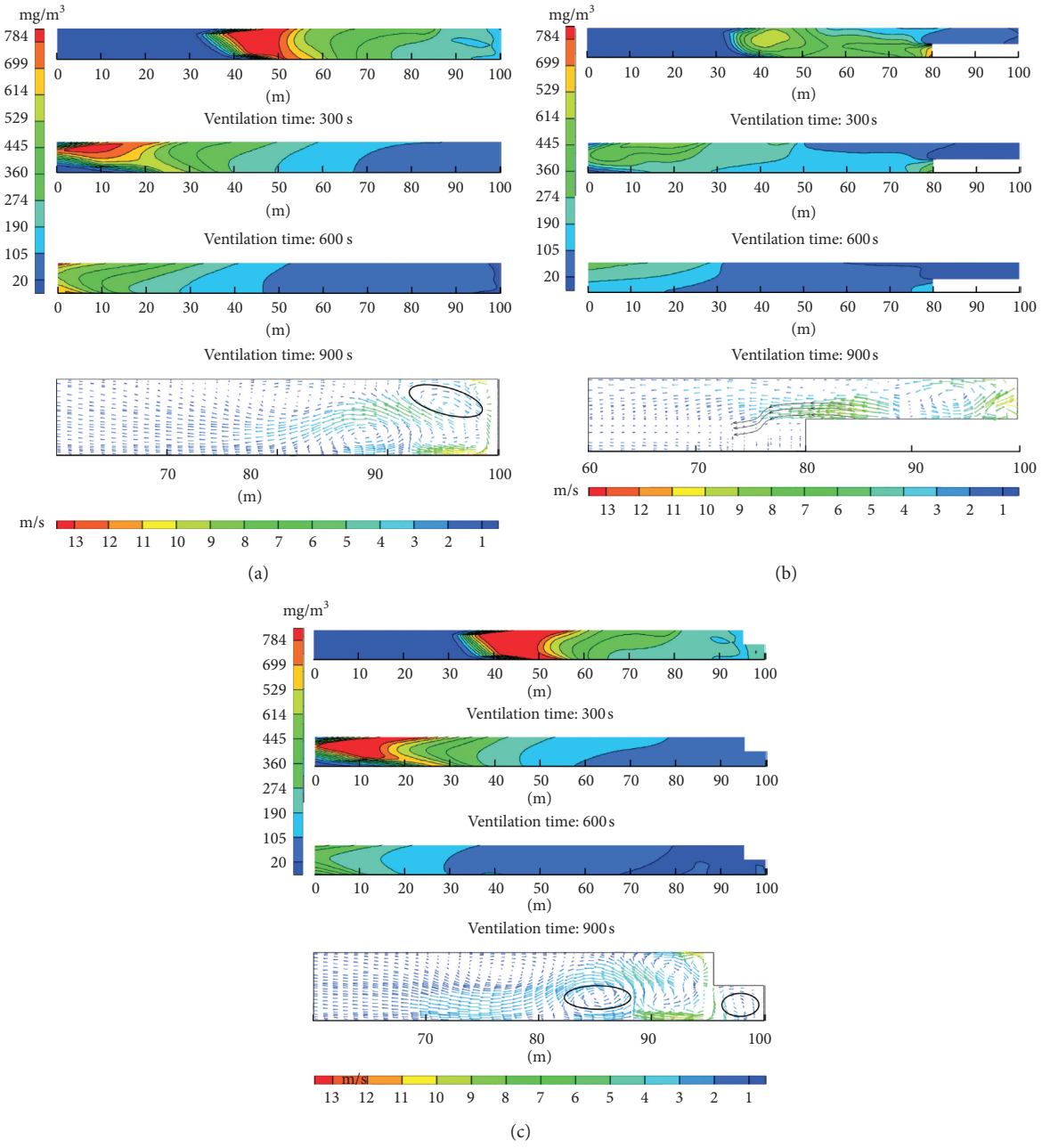

Figure 11: CO ventilation diffusion concentration change in the tunnel after blasting cloud map and working face speed vector. (a) Full-section construction. (b) Step construction. (c) Advance construction of lower guide tunnel.

method (as shown in Figure 11(b)), the jet air impacts the bottom surface of the step and changes direction. Its trajectory moves in a parabolic shape toward the exit of the tunnel, resulting in a dilution dead zone on the lower step. When the lower guide tunnel is used in advance construction (as shown in Figure 11(c)), there are vortex zones in front of the lower guide tunnel and in front of Palm face. During the ventilation stage, CO retention occurs near these two parts.

5. Conclusions

In this paper, based on the actual working conditions of HD3K0 + 148 section of No. 3 horizontal tunnel of Yuelongmen Tunnel, the CO concentration variation and diffusion characteristics of the tunnel after drilling and blasting construction are simulated, and the following conclusions are drawn through analysis:

(1) The airflow model of the Navier–stokes equation and the RNG $k-\varepsilon$ turbulence model are established based on the assumption of tunnel ventilation flow, so as to achieve the dynamic simulation of CO diffusion in 3D space.

(2) It is found after the comparison of air pipe layout methods that when the air pipe is laid near the wall at the tunnel vault, the CO near the tunnel face could reach the standard limit in the shortest time, which will decrease to the standard limit after ventilation for 588 s, but it will take 738 s, 840 s, and 786 s if the air pipe is laid at the corner, haunch, and center, respectively. When the air pipe is laid at the tunnel vault, CO is easy to gather at the bottom of the tunnel face and vault, which has the least impact on the occupational health of construction workers because this position is far away from the worker's breathing height.

(3) Benching tunneling method could effectively reduce the retention time of CO near the tunnel face, and the CO concentration on the tunnel face decreases to the standard limit after ventilation for 326 s, while 847 s and 784 s is required for the full-face tunneling method and lower pilot heading method, respectively. In addition, when the full-face tunneling method and lower pilot heading method are used for construction, ventilation will easily cause CO to be retained in the gap between the inner wall of the tunnel and the air pipe.

Data Availability

The data used to support the findings of this study are available from the corresponding author upon request.

Conflicts of Interest

The authors declare that they have no conflicts of interest.

Acknowledgments

This work was supported by the Fundamental Research Funds for the National Natural Science Foundation of China (51779197, 51979208, and 51774222), the Postdoctoral Innovation Research Post of Hubei Province of China (20201jb001), the Hubei Key Laboratory of Roadway Bridge and Structure Engineering (Wuhan University of Technology) (no. DQJJ201904), the Fundamental Research Funds for the Central Universities (WUT: 2019IVA098), and the Youth Talent Project of Science and Technology Research Program of Hubei Provincial Department of Education (Q20192801).

References

[1] D. Vasovic, S. Kostic, M. Ravilic et al., "Environmental impact of blasting at drenovac limestone quarry (Serbia)," *Environmental Earth Science*, vol. 72, no. 10, pp. 3915–3928, 2014.

[2] A. Jafar, B. Ezzeddin, and N. Hadi, "Green biocompatible approach to reduce the toxic gases and dust caused by the blasting in surface mining," *Environmental Earth Sciences*, vol. 75, no. 3, pp. 191–203, 2016.

[3] S. Torno and J. Toraño, "On the prediction of toxic fumes from underground blasting operations and dilution ventilation. conventional and numerical models," *Tunnelling and Underground Space Technology*, vol. 96, Article ID 103194, 2020.

[4] R. Huang, X. Shen, B. Wang, and X. Liao, "Migration characteristics of CO under forced ventilation after excavation roadway blasting: a case study in a plateau mine," *Journal of Cleaner Production*, vol. 267, Article ID 122094, 2020.

[5] A. Moen, L. Mauri, and V. D. Narasimhamurthy, "Comparison of $k-\varepsilon$ models in gaseous release and dispersion simulations using the CFD code FLACS," *Process Safety and Environmental Protection*, vol. 130, pp. 306–316, 2019.

[6] O. Raaschou-Nielsen, Z. J. Andersen, S. S. Jensen et al., "Traffic air pollution and mortality from cardiovascular disease and all causes: a danish cohort study," *Environmental Health*, vol. 11, no. 1, pp. 60–67, 2012.

[7] M. G. Vega, K. M. Argüelles Díaz, J. M. Fernández Oro, R. B. Tajadura, and C. Santolaria Morros, "Numerical 3D simulation of a longitudinal ventilation system: memorial tunnel case," *Tunnelling and Underground Space Technology*, vol. 23, no. 5, pp. 539–551, 2008.

[8] F. Wang and M. Wang, "A computational study on effects of fire location on smoke movement in a road tunnel," *Tunnelling and Underground Space Technology*, vol. 51, pp. 405–413, 2016.

[9] Editorial Department of China Journal of Highways, "Summary of academic research on tunnel engineering in China·2015," *Chinese Journal of Highways*, vol. 28, no. 5, pp. 1–65, 2015.

[10] W. Pang, H. L. Fu, W. Pei et al., "Real-time monitoring of harmful gas components in ventilation and construction environment of Tianmushan tunnel," *Modern Tunnel Technology*, vol. 56, no. 1, pp. 150–158, 2019.

[11] M. Sambolek, "Model testing of road tunnel ventilation in normal traffic conditions," *Engineering Structures*, vol. 26, no. 12, pp. 1705–1711, 2004.

[12] F. Cascetta, M. Musto, and G. Rotondo, "Innovative experimental reduced scale model of road tunnel equipped with realistic longitudinal ventilation system," *Tunnelling and Underground Space Technology*, vol. 52, pp. 85–98, 2016.

[13] Y. Li, L. Ling, and J. Chen, "Combined grey prediction fuzzy control law with application to road tunnel ventilation system," *Journal of Applied Research and Technology*, vol. 13, no. 2, pp. 313–320, 2015.

[14] E. Karaka, "The control of highway tunnel ventilation using fuzzy logic," *Engineering Applications of Artificial Intelligence*, vol. 16, no. 7-8, pp. 717–721, 2003.

[15] K. Wu, Q. M. Yang, C. Kang et al., "Adaptive critic design based control of tunnel ventilation system with variable jet speed," *Journal of Signal Processing Systems*, vol. 86, no. 2-3, pp. 269–278, 2017.

[16] F. Wang, M. Wang, and Q. Wang, "Numerical study of effects of deflected angles of jet fans on the normal ventilation in a curved tunnel," *Tunnelling and Underground Space Technology*, vol. 31, pp. 80–85, 2012.

[17] I. Diego, J. S. Toraño, and M. GentMenéndez, "A practical use of CFD for ventilation of underground works," *Tunnelling and Underground Space Technology*, vol. 26, no. 1, pp. 189–200, 2011.

[18] C. D. Ang, G. Rein, J. Peiro, and R. Harrison, "Simulating longitudinal ventilation flows in long tunnels: comparison of full CFD and multi-scale modelling approaches in FDS6," *Tunnelling and Underground Space Technology*, vol. 52, pp. 119–126, 2016.

[19] J. Toraño, S. Torno, M. Menendez, M. Gent, and J. Velasco, "Models of methane behaviour in auxiliary ventilation of underground coal mining," *International Journal of Coal Geology*, vol. 80, no. 1, pp. 35–43, 2009.

[20] C. Nan, J. Ma, Z. Luo, S. Zheng, and Z. Wang, "Numerical study on the mean velocity distribution law of air backflow and the effective interaction length of airflow in forced ventilated tunnels," *Tunnelling and Underground Space Technology*, vol. 46, pp. 104–110, 2015.

[21] S. Zheng, J. Toraño, M. Ulecia, and C. Allende, "Conventional and numerical models of blasting gas behaviour in auxiliary ventilation of mining headings," *Tunnelling and Underground Space Technology*, vol. 34, no. 34, pp. 73–81, 2013.

[22] M. Ichinose, S. Nakayama, K. Uchino, and M. Inoue, "In-situ measurement and simulation by CFD of methane gas distribution at a heading faces," *Shigen-to-Sozai*, vol. 114, pp. 769–775, 1998.

[23] S. Nakayama, K. Uchino, and M. Inoue, "Analysis of ventilation air flow at heading face by computational fluid dynamics. analysis of environmental conditions at heading face with auxiliary ventilation. (1st report)," *Shigen-to-Sozai*, vol. 111, no. 4, pp. 225–230, 1995.

[24] K. Zhang, Y. Cao, H. G. Ji et al., "Experimental study on the emission law and concentration prediction model of gun smoke in the single head roadway," *Modern Tunnel Technology*, vol. 51, no. 4, pp. 150–154, 2014.

[25] Y. Cao, H. G. Ji, and Q. M. Zhou, "Calculation of smoke exhaust time after blasting in roadway," *Journal of Harbin Institute of Technology*, vol. 49, no. 8, pp. 135–140, 2017.

[26] H. Herwig, D. Gloss, and T. Wenterodt, "A new approach to understanding and modelling the influence of wall roughness on friction factors for pipe and channel flows," *Journal of Fluid Mechanics*, vol. 613, no. 6, pp. 35–53, 2008.

[27] S. G. Kandlikar, "Roughness effects at microscale reassessing nikukadse's experiments on liquid flow in rough tubes," *Bulletin of the Polish Academy of Sciences Technical Sciences*, vol. 53, no. 4, pp. 343–348, 2005.

[28] Y. Hu, C. Werner, and D. Li, "Influence of the three-dimensional heterogeneous roughness on electrokinetic transport in microchannels," *Journal of Colloid and Interface Science*, vol. 280, no. 2, pp. 527–536, 2004.

[29] *Technical Guide for Railway Tunnel Construction (TZ204-2008)*, China Railway Publishing House, Beijing, China, 2008.

[30] J. W. Tan, V. Garaniya, T. Baalisampang et al., "Modeling impacts of combustion products on humans in complex processing facilities," *Process Safety Progress*, vol. 39, no. S1, Article ID e12114, 2020.